A lipoprotein partner for the *Escherichia coli* outer membrane protein TolC

Jim Horne*, Elise Kaplan*[+], Ben HS Jin, Emmanouela Petsolari, Jan M. Gradon[++], Yvette Ntsogo, Andrzej Harris, Dingquan Yu, Ben F. Luisi

Department of Biochemistry, University of Cambridge, Tennis Court Road, Cambridge CB2 1GA, UK

[+]current address, Molecular Microbiology and Structural Biochemistry (MMSB), UMR 5086 CNRS/University of Lyon, Lyon, France

[++]current address, School of Biochemistry, Faculty of Life Sciences, University of Bristol, Bristol BS8 1TD, United Kingdom

*equal contributions

Abstract

The outer-membrane protein TolC from *Escherichia coli* belongs to an extensive superfamily whose members are found throughout the didermal, Gram-negative bacterial lineages. The protein serves as an activated exit duct in multi-drug efflux pumps and protein secretion machinery. Many TolC homologs bear a lipid modification on the N-terminus that embeds into the inner leaflet of the outer membrane and appears to have been a conserved feature for millions of years; however, the moiety is absent entirely in the *E. coli* TolC. We have discovered that the *E. coli* lipoprotein YbjP interacts extensively with the periplasmic surface of TolC and its N-terminal lipid moiety is embedded in the membrane, mimicking the intramolecular interactions seen for related proteins. Here, we present cryo-EM structures of the MacA-MacB-TolC and AcrA-AcrB-TolC tripartite pumps complexed to YbjP. We demonstrate that the association occurs spontaneously both *in vitro* and *in vivo* and that YbjP facilitates recovery following exposure to bacteriostatic agents. We suggest that the YbjP-TolC interaction may facilitate the assembly of the outer membrane protein in a redundant biogenesis pathway.

Keywords: multi-drug efflux pump, MacAB-TolC, AcrABZ-TolC, type I secretion, lipoprotein, membrane protein assembly

INTRODUCTION

The bacterial cell envelope is a highly complex compartment and protective barrier against the external environment, ensuring survival in response to chemical threats while maintaining individual cellular identity and communication of signals within communities. In Gram-negative species, including clinical pathogens such as *Escherichia coli*, *Pseudomonas aeruginosa, Haemophilus influenzae*, and *Helicobacter pylori*, the envelopes are characterised

by an organisation of two lipid bi-layer membranes and an interstitial partition, referred to as the periplasm, that encompasses a peptidoglycan sacculus conferring mechanical robustness (Guest and Silhavy, 2023; Gumbart et al., 2021). The envelope is home to a diversity of dedicated machineries that selectively move molecules across the barrier facilitated by energy transduction. Harmful compounds such as antibiotics and bactericidal agents as well as effector proteins are displaced through this barrier by energy-dependent machines, and representative and well-characterised examples are the tripartite assemblies AcrA-AcrB-TolC and MacA-MacB-TolC of *E. coli*, which are powered respectively by proton motive force and ATP binding and hydrolysis (Du et al., 2018). The AcrA-AcrB-TolC assembly drives efflux of chemically diverse compounds, and MacA-MacB-TolC can transport macrolides, peptide toxins and host antibacterial peptides (Honeycutt et al., 2020; Zhang et al., 2025). Structures of these and analogous assemblies have provided insight into how the machines operate to recognise and move complex transport substrates in a preferred direction against concentration gradients (Du et al., 2018; Wang et al., 2017; Glacier et al., 2020; Tsutsumi et al., 2019; Fitzpatrick et al., 2017).

The outer membrane component of the efflux assemblies, TolC, is a homotrimeric protein with a self-closing β-barrel topology that inserts into the outer membrane and a long helical structural domain that interacts with periplasmic partners such as AcrA or MacA (Figure 1A). TolC homologs are found throughout diderm bacteria, highlighting the functional importance of this superfamily (Stubenrauch et al., 2022). The long helical portion of TolC can be subdivided into an α-helical barrel domain, which appears to be a stable structural unit (Calladine et al., 2001; Huang et al., 2014), and conventional coiled-coil segments that dilate from a sealed resting state to an open-state when interacting with a periplasmic partner (Wang et al., 2017). At the junction of the two helical regions, a meander forms a circumferential ring known as the equatorial domain and is proposed to interact with the peptidoglycan layer of the periplasm (Shi et al., 2019).

Here, in our analysis of the MacA-MacB-TolC tripartite assembly, we observed unexpected cryo-EM density spanning between the equatorial domain of TolC and the transmembrane boundary. Using a structural topology pattern recognition query against predicted folds of *E. coli* proteins, we identified the protein as a lipoprotein of unknown function, YbjP (UniProt ID P75818). The N-terminus of YbjP trails over the surface of TolC to reach the outer membrane where the lipoprotein lipid moiety is embedded. Our results do not support an allosteric or

signalling role for YbjP but suggest that the lipoprotein is required for fitness under certain membrane stress conditions. We propose that YbjP may facilitate the biogenesis of TolC during times of rapid adaptation.

RESULTS

Cryo-EM structure of TolC bound to a lipoprotein

Earlier cryo-EM work on the MacA-MacB-TolC assembly used samples reconstituted in detergents (Fitzpatrick et al. 2017). We explored preparation of MacA-MacB-TolC in peptidiscs as a better mimic of the membrane environment (Carlson et al., 2018). From these preparations, we were able to solve the structure by cryo-EM with high-quality density for all three components of the assembly. In one of our preparations, additional density was observed near the equatorial domain of TolC, extending towards the outer membrane β-barrel domain (Figure 1B). We refined this structure to a final resolution of 2.48 Å (Supplemental Figure S1 and Table S1) and fitted the additional density with secondary structural elements (Figure 1C). The incomplete candidate fold was then searched against the database of *E. coli* protein structures predicted by AlphaFold2 (Jumper *et al*., 2021) using the DALI topology recognition program (Holm, 2022). The result matches well with the lipoprotein YbjP (P75818) which could be fitted into the cryo-EM map. The refined model is presented in Figure 1D. The lipoprotein globular domain is formed by a series of four consecutive α-helices (α1-α4), followed by four antiparallel β-strands (β1-β4) and a C-terminal α-helix (α5) (Figure 1E). Structural alignment of the predicted YbjP and cryo-EM refined models reveals a strikingly high degree of similarity (rmsd 0.53 Å over 118 residues), confirming the accuracy of the prediction (Figure 1D, *insert*).

Interactions between TolC and lipoprotein YbjP

YbjP straddles two adjacent TolC protomers, and the interface is stabilised by multiple hydrogen bonding and ionic interactions involving the linker and globular domain of YbjP and two TolC subunits (Figure 2A). The intermolecular contacts engage almost 20 residues in both TolC and YbjP. The lipoprotein flexible linker runs along TolC N-terminal helix from the equatorial to the transmembrane domains and is stabilised by several hydrogen bonds involving N32, R35, R24, Y98 and L17 from one TolC monomer (Figure 2A, panel 1). This cluster is

consolidated by hydrogen bonding interactions between S107, S109, T110 and N113 from YbjP loop connecting beta-strands β1 and β2 and R234, Q306 and Y307 from the proximal adjacent TolC monomer, maintaining this flexible loop perpendicular to the lipoprotein linker. YbjP D115 and N118 also make contacts with R18 and E314 from TolC.

Interestingly, the YbjP globular domain is strongly associated via a cluster of ionic interactions (Figure 2A, panel 2), mediated by a trio of positive, negative, positive residue (R122, E135, R151) which each contacts residue of opposite charge in TolC (D231, R227, E317). Finally, numerous hydrogen bonds are formed between YbjP globular domain and helices from both TolC monomers (Figure 2A, panel 3) engaging G155, V157 and A159 backbones, and K70, N118, E135 and R151 side chains from the lipoprotein. Residue conservation of YbjP was evaluated visually with the server CONSURF, revealing that the conserved residues are located at the interface with TolC (Figure 2B).

Like other lipoproteins, YbjP is predicted to be processed by cleavage of the signal sequence at residue C19 (also referred as to the +1 Cys of the matured lipoprotein), then lipidated as N-palmitoyl and S-diacylglycerol cysteine. These processing and modification steps are likely to occur at the inner membrane (Guest and Silhavy, 2023). Although the density is not well defined for the lipid moiety due to its flexibility, the map does reveal a portion of the hydrocarbon embedded into the inner leaflet of the outer membrane. This is consistent with mass spectrometry studies that have identified YbjP as an outer membrane protein (Molloy et al., 2000). Interestingly, there is no density for the lipoprotein R3 acyl chain suggesting that the cysteine α-amino group has not been modified while *E. coli* lipoproteins are presumed to be tri-acylated to traffic via the Lol system (May and Grabowicz, 2025; Noland et al., 2017). Further clarification is needed to establish if YbjP is naturally di- or tri-acylated.

TolC-YbjP interaction in the AcrA-AcrB-AcrZ-TolC assembly

Cryo-EM analysis of reconstituted AcrABZ-TolC-YbjP assembly shows that the YbjP forms the same interactions in both the MacAB-TolC and AcrABZ-TolC (Supplementary Figure S2A, B). The AcrABZ-TolC-YbjP assembly was also reconstituted into peptidoglycan, and the position of the peptidoglycan layer between AcrA and TolC corresponds with the localization previously inferred from low-resolution cryo-ET data (Shi *et al*., 2019) (Supplementary Figure S2C-E). The reconstructed maps indicate that the YbjP may not interact with the peptidoglycan

layer, but this cannot be certain due to the limited resolution of the cryo-EM map. *In vitro* characterizations indicated that YbjP can interact with peptidoglycan in pull-down assays, but this is likely to be non-specific as alanine substitutions in the domain proximal to the peptidoglycan (R80, D81, R85 and E86) had little impact on the efficiency of the pull-downs. Photo-crosslinking in substitutions of the photoreactive amino acid para-benzophenone (pBPA) at positions D77, Q166, E169 and R171 did not give evidence for peptidoglycan linked species. The data suggest that YbjP may not form avid interactions with the peptidoglycan.

Validation of the TolC-YbjP interaction by in vitro pull-down and in vivo photo-crosslinking

To validate the TolC-YbjP interactions, we used an *in vitro* affinity pull-down assay using purified proteins. For this, we produced a soluble mutant of YbjP, hereafter referred to as $YbjP_s$, removing the lipobox conserved cysteine that carries the acyl chains, and the 8 following residues corresponding to a flexible linker joining the acylated cysteine to the protein globular domain. The protein (D28-R171) bearing a N-terminal his-tag was purified from the cytoplasm and immobilised on nickel resin. As shown in Figure 3A, detergent-purified TolC remained attached to the resin only in the presence of $YbjP_s$ confirming the association between the two proteins and demonstrating that the lipoprotein lipid moiety is not required for the interaction to occur. We were not able to detect an interaction between $YbjP_s$ and Pal (peptidoglycan associated protein) lipoprotein or between Pal and TolC using the pull-down assay.

Interactions between TolC and $YbjP_s$, were also measured by isothermal titration calorimetry. Results are presented in Figure 3B and in Supplementary Table S3. The binding event is exothermic, consistent with electrostatic interactions at the protein-protein interface. The dissociation constant is in the micromolar range ($K_D \sim 4$ μM). Although this value represents a weak to moderate association, the affinity is likely to be substantially greater in the presence of the lipid modification, which will localise YbjP and decrease the configurational entropy for TolC interaction. Moreover, the YbjP 8-residue linker joining the lipid modification to the protein globular domain is absent here but participates in TolC interaction (Figure 2A, panel 1).

To further validate if YbjP interacts with TolC in the cell, we engineered amber mutants of full-length, histidine-tagged YbjP. We introduced a plasmid coding for each amber variant in *E. coli* C43 cells transformed with the pEVOL vector for incorporation of the unnatural amino acid

para-benzophenone, pBPA (Chin et al. 2002, Young et al. 2009). Guided by our YbjP-TolC structure, we replaced residues located either at the protein-protein interface (T110, N113) or at a distance (N43, N90 and H104) as negative controls. To validate the experiment, we also constructed amber mutants of histidine-tagged AcrA, an inner membrane protein known to interact with TolC, and substituted Q136 and Y137, two residues proximal to TolC in the AcrABZ-TolC efflux pump structure (Wang et al. 2017). Cells were grown in a media supplemented with pBPA, induced by addition of IPTG and arabinose and then irradiated for 15 min with UV. After cell lysis, his-tagged proteins were retrieved from the samples by affinity chromatography. Control cultures were either not supplemented with pBPA or not UV treated. Purified fractions were analyzed by SDS-PAGE and immunoblotting (Figure 3C). We observed covalent photo-adducts that migrate at higher molecular weight compatible with AcrA-TolC or YbjP-TolC adducts only for the pBPA-supplemented cells and only after illumination with UV light for the residues that are proximal to the TolC surface, but not those that are distal. These results are consistent with a model for YbjP lipoprotein interactions with TolC *in vivo*.

Evolutionary profile of YbjP

To infer the function of YbjP, we investigated its evolutionary profile. In the PFAM database, YbjP is annotated to contain one DUF3828 domain. The most well-characterized DUF3828-containing protein is Tai3, a periplasmic type IV cognate immunity protein of the T6SS amidase effector Tae3 (Russel et al., 2012; Dong et al., 2013). Another periplasmic protein YqhG contains one full and one partial DUF3828 domain and is involved in regulating type I fimbriae expression in *E. coli* by an unknown mechanism (Bessaiah et al., 2019). Structural alignment of YbjP with the Tai3 crystal structure and YqhG AlphaFold prediction are shown in Figure 4A.

To investigate whether YbjP is functionally homologous to Tai3 or YqhG, we reconstructed a phylogenetic history of the DUF3828-containing proteins, which could be classified into three major families based on taxonomy, gene synteny, presence of a signal peptide and a conserved QDX motif, involved in Tae3 inhibition (Supplementary Table S4). The result indicates that the function of YbjP is likely distinct from that of Tai3 or YqhG (Figure 4B). We noted that Tai3 is found in a broader range of bacterial groups (Gammaproteobacteria, Betaproteobacteria, and Bacteroidota/Chlorobiota) compared to YbjP. Similarly, YbjP is restricted to some members of the Enterobacterales Order within the class of Gammaproteobacteria, unlike TolC which is more widespread (Supplementary Figure S3). Notably, the TolC-YbjP interface is

more conserved in Enterobacterales with YbjP than without (Figure 4C), suggesting a scenario where YbjP evolved recently from an ancestral Tai3-like protein to become a TolC interactor.

YbjP is not required for TolC insertion into the outer membrane

Outer membrane efflux proteins structurally homologous to TolC often carry a N-terminal acylation. This is the case for the drug exit duct OprM in *Pseudomonas* and the outer membrane efflux proteins in *E. coli* MdtP, MdtQ, and CusC, but with the notable exception of TolC. The reason for the presence or absence of acylation remains unclear, but it has been proposed that acylation has roles in anchorage to the membrane and in membrane insertion. We first postulated that YbjP could compensate for the absence of lipid modification in TolC. Indeed, YbjP linker and N-acetylation mimics the linker and acetylation arrangement seen in OprM and CusC (Figure 5A). Similarly, AlphaFold3 predicted the interaction of YbjP with TolC but not with the other outer membrane efflux proteins that are lipoylated in *E. coli* (Figure 5B). Consistent with this, we found that *E. coli* TolC is distinct from its lipoylated structural homologues (Figure 5C), suggesting the possibility that YbjP evolved to compensate for the absence of lipidation.

To explore this hypothesis, we obtained an Δ*ybjP E. coli* strain from the Keio collection and prepared periplasmic, inner and outer membrane extractions. Each fraction was then subjected to immunoblotting using anti-TolC antibodies. Although the outer membrane is the final destination for TolC, a fraction of the protein is expected to be in the inner membrane during the early stages of biogenesis. We did detect the protein in both membrane compartments but not in the periplasmic fraction. No difference in the location of TolC in either the inner or outer membrane compartment was observed when comparing the Δ*ybjP* and the parental strains (Figure 5D) in presence or absence of chloramphenicol. Moreover, additional bioinformatic analysis reveals that while most organisms containing the *ybjP* gene possess non-lipoylated TolC, non-lipoylated TolC is also present in most organisms lacking *ybjP* (Figure 5E). Altogether, this indicates that YbjP may not be necessary to compensate for the lack of lipoylation.

Exploring in vivo function of YbjP

YbjP is annotated as a protein of unknown function, but it has been noted that the gene product of *ybjP* may either directly, or indirectly, be a global regulator of carbon metabolism (Bergès

et al., 2021) with impact on motility (Tenorio et al., 2003). Previous RNA-seq analysis show the upregulation of *ybjP* in response to membrane-disrupting chemicals, including vanillin (Pattrick et al., 2019) and EDTA (Janssens et al., 2023). Moreover, *Klebsiella pneumoniae* (strain Ecl8) Δ*ybjP* has been reported to be more resistant than the parental strain to novobiocin (4-fold increase in MIC) (Miller, 2023), which is a DNA gyrase inhibitor and substrate of AcrAB-TolC (Abdali et al., 2017). The outer membrane protein SlyB has been shown to encapsulate TolC during stress (Janssens *et al*. 2023), and 2D classification images of TolC-SlyB indicate that SlyB binds at the TolC-YbjP interface. Indeed, the AlphaFold3 structure of TolC-SlyB predicts the binding of SlyB at the TolC-YbjP interface (Supplementary Figure S4). Since both YbjP and TolC are upregulated in response to EDTA treatment (Janssens *et al*., 2023), YbjP and SlyB might compete for TolC under conditions of outer membrane stress.

We explored different stress situations to identify conditions in which the YbjP null strain had a clear growth defect compared to the parental strain. A Δ*tolC* strain was also tested as a positive control. There was little impact of high temperature (42°C) or the presence of high salt (1 M NaCl) on growth on nutrient-agar plates, as seen in a dilution series (Figure 6A) while the Δ*tolC* strain was sensitive to the high salt condition. However, this was mildly accentuated in the presence of the cationic detergent benzalkonium chloride (BZK), which is a substrate for the AcrABZ-TolC pump, while no effect was observed on the Δ*ybjP* cells with BZK alone. We then evaluated the immediate response of the YbjP null strain to BZK in liquid culture (Figure 6B). A small growth defect (~20% after 8h culture) was observed in Δ*ybjP* cells in the absence of compound compared to WT cells, but the presence of BZK led to a significant growth defect in the YbjP null strain, with an optical density reaching ~85% of the WT cell level after 8h culture. This suggests that YbjP plays a role in the rapid adaptation of cells to noxious compounds.

DISCUSSION

Our structural and functional results indicate that the lipoprotein YbjP is located in the outer membrane, where it can interact with the outer membrane protein TolC. The mode of interaction between TolC and YbjP resembles closely the intramolecular interactions of the lipoylated N-terminus in TolC paralogs, such as OprM from *Salmonella*. The interaction is likely functionally important within some Enterobacterales. It is proposed that the TolC archetype may bear sequence or environmental features that have limited its distribution, or it is a more

recently evolved form in the TolC-like protein family (Stubenrauch et al., 2022). It is possible that TolC and YbjP co-evolved in this lineage.

The biogenesis of TolC presents intriguing mechanistic puzzles. The insertion stage of outer membrane proteins involves the β-barrel assembly machine (BAM) complex (Voulhoux et al., 2003; Wu et al., 2005), but the process is not well characterised for a non-canonical porin-like protein with an extended hydrophilic portion, such as TolC, nor are the earlier steps of translocation across the periplasm. The chaperone translocation and assembly machinery (TAM) facilitates assembly of TolC into the outer membrane in a potentially redundant pathway (Stubenrauch et al., 2022). Reflecting on the potential requirements suggests key aspects to consider for understanding the process. First, the protomers must be moved across the periplasm from the translocon where the nascent chains emerge. Second, this insertion would be coordinated to deliver three protomers to fold into the full trimeric architecture. Lastly, the folding does not require exogenous energy and is likely driven by hydrophobic interactions with the highly crowded and asymmetric lipid bilayer (Horne et al., 2020).

Mechanistic puzzles also arise when considering how lipoproteins such as OprM and YbjP arrive at the outer membrane and are inserted. Lipoproteins are processed and lipid groups are attached to a conserved cysteine residue that immediately follows the signal sequence in the inner membrane (Guest and Silhavy, 2023). Acylated thiols are found in components of other bacterial efflux assemblies. The structure of CusC indicates the presence of an acylated thiol on the N-terminal cysteine, and acylation is also found in CmeC, but nothing has been found to be added to the N-terminal cysteine of the MtrE structure. Post-translational lipidation is particularly essential for the secretion and localization of some membrane proteins, a process involving different acyl transferases (Aicart-Ramos et al., 2011; Linder and Deschenes, 2007; Kovacs-Simon et al., 2011; Nakayama et al., 2012). Why proteins that are embedded within cellular membranes via a large hydrophobic structural domain need modifications such as the N-terminal lipidation appears puzzling. Akama et al. (2004) suggested that these proteins must first be anchored to the membrane by an N-terminal lipid so that the insertion of their large hydrophobic domain may be triggered. Structural evidence indicates that this later step is critical for the correct folding of outer membrane factors (OMFs) and highlight the possible involvement of membrane-interacting components in the OMF opening process and consequently the efflux-pump function (Lei et al., 2014).

Translocation of lipoprotein to the outer membrane in *E. coli* requires five essential proteins (LolA-E) (Guest and Silhavy, 2023). The mechanism involves lipoprotein extraction from the inner membrane by the ABC transporter LolCDE prior to transfer to the periplasmic carrier LolA. In turn, LolA delivers the lipoproteins to the outer membrane acceptor LolB, which facilitates their insertion into the outer membrane. It is envisaged that this pathway is involved in the movement of OprM and its lipidated outer membrane homologs. As *E. coli* TolC is not lipoylated, it is possible that YbjP acts as a chaperone that intercepts the TolC and aids its translocation across the periplasm via the Lol system. However, this proposed pathway is likely redundant or not essential, as TolC is still found in the outer membrane in strains null for YbjP. The BAM complex impacts on TolC assembly in *E. coli* (Werner et al., 2005; Malinverni et al., 2006), but surprisingly it is not involved in assembly of the TolC-like proteins OprM in *P. aeruginosa* (Hoang et al., 2011). The pathway for insertion is likely to be redundant and divergent for the TolC family (Stubenrauch et al., 2022). Notably, a broad screen of cell envelope protein complexes in *E. coli* did not identify physical or genetic interactions between the YbjP and TolC (Babu et al., 2017), but such interactions were found between YbjP and the partners of TolC in the tripartite assembly, namely the RND transporter AcrB and the periplasmic AcrA. It may be that the interactions between TolC and YbjP *in vivo* are weak and transient, as might occur for example during TolC insertion into the outer membrane. Our structural data indicates that YbjP and SlyB bind to the same region of TolC, suggesting they may compete for interaction in a complex regulatory network that responds to environmental stress.

Our *in vivo* analysis of YbjP function (Figure 6) revealed a potential role in helping bacteria adapt to stressful conditions, such as exposure to the detergent benzalkonium chloride (BZK). In the presence of BZK, *ybjP* knockout cells (Figure 6B) showed a significantly reduced growth rate compared to the wild-type strain. However, in the absence of the detergent, the knockout strain grew at a rate comparable to wild-type *E. coli* exposed to BZK, and where the detergent is actively removed by efflux pumps. These findings suggest that YbjP plays a role in regulating bacterial growth and coordinating cell division under membrane stress conditions. We propose that YbjP supports the clustering and partitioning of transport machineries during cell division or during stress (Zhang et al., 2025), thereby influencing how efficiently bacteria adapt to environmental conditions. Furthermore, we hypothesize that YbjP contributes to membrane

stress responses by interacting with TolC, potentially facilitating the assembly of outer membrane proteins via a redundant pathway.

MATERIALS AND METHODS

Preparation of disulphide-engineered MacAB-TolC and reconstitution into peptidisc

E. coli BL21 (DE3) strain was transformed with plasmids pET20b-hexaHis-$MacA_{D271C}$-$MacB_{G465C}$ expressing the $MacA_{D271C}$ and $MacB_{G465C}$ mutants, allowing a disulphide link, with a C-terminal hexaHis-tag on MacB and pRSFduet-TolC-FLAG expressing full-length TolC with a C-terminal FLAG-tag (Fitzpatrick *et al*., 2017). Transformed cells were spread onto LB agar plates containing 50 µg mL^{-1} carbenicillin and 50 µg mL^{-1} kanamycin and were incubated at 37°C overnight. A single colony was used to inoculate 50 mL of LB medium containing 50 µg mL^{-1} carbenicillin and 50 µg mL^{-1} kanamycin. The preculture was grown at 37°C, with an orbital shaker set at 200 rpm for 4 h. When the absorbance at 600 nm reached between 0.5 and 0.7, the preculture was used to inoculate 6 L of 2YT medium containing 50 µg mL^{-1} carbenicillin and 50 µg mL^{-1} kanamycin in 6x2 L baffled flasks. Bacteria were grown at 37°C, 200 rpm until OD_{600nm} reached 0.5 and were subsequently induced with 0.25 mM isopropyl β-d-1-thiogalactopyranoside (IPTG). The culture was further incubated at 20°C, 200 rpm overnight. Cells were collected by centrifugation (5,000 *g* for 30 min at 4˚C) and pellets were resuspended in a buffer containing 20 mM Tris-HCl pH 8.0 and 400 mM NaCl (Buffer A).
One tablet of EDTA-free protease inhibitor per 50 mL, 5 µg mL^{-1} lysozyme and 5 U mL^{-1} DNase I were added to the cell suspension and incubated 1 h at 4°C. The mixture was then passed five times through a water-cooled high-pressure homogeniser (Emulsiflex), keeping the pressure below 14,500 psi throughout. The resulting lysate was centrifuged (9,000 *g*, 30 min, 4˚C) to remove cell debris and then ultracentrifuged (175,000 *g*, 4 h, 4˚C) to pellet membranes.

Membranes were solubilized in 50 mL of buffer 20 mM Tris pH 8.0, 400 mM NaCl with 1.5% (wt/v) β-dodecyl maltoside (β-DDM) and one tablet of EDTA-free protease inhibitor for 3 h at 4°C with gentle stirring. The solution was then purified by Ni-NTA chromatography after addition of 10 mM imidazole. The elution peak was further purified with ANTI-FLAG M2 affinity resin (0.5 mL, Sigma Aldrich), pre-equilibrated with buffer A supplemented with 0.05%

wt/v β-DDM. The elution fraction was added to the resin and incubated at 4°C for 1 h with gentle agitation. The sample was then washed with buffer A containing 0.05% β-DDM and then 0.03% (wt/v) decyl maltose neopentyl glycol (DMNG). Peptidisc (Carlson et al., 2018) at 1 mg mL^{-1} in 400 mM Tris-HCl and additional *E. coli* lipid (100 µL at 20 mg mL^{-1}) were added to the column. After 16h at 4°C, the resin was washed with buffer A containing no detergent and then eluted with 3xFLAG peptide (Sigma-Aldrich). Flow-through was collected at each step and analysed by SDS-PAGE. The presence of the full assembly was confirmed by mass photometry (Refeyn).

MacAB-TolC-YbjP cryo-EM sample preparation and data collection

For single-particle cryo-EM structure solution, the samples of MacAB-TolC-YbjP complex reconstituted in peptidisc (Carlson et al., 2018) were thawed and diluted to 0.5 mg mL^{-1} in a buffer composed of 20 mM Tris pH 8.0, 100 mM KCl, 2 mM TCEP and 1 mM NaN_3. A 3-µL aliquot of dilute protein was applied onto a Cu 300-mesh EM grid layered with R1.2/1.3 holey carbon support film (Quantifoil Micro Tools, GmbH), which had been glow-discharged immediately prior to use. The sample deposited on the EM grid was blotted of excess solution and vitrified in liquid ethane using Vitrobot Mark IV (Thermo Fisher Scientific, Inc.) robotic cryo-EM plunger.

The grids were imaged using Titan Krios G3 transmission electron microscope (Thermo Fisher Scientific Inc.) operating at accelerating voltage of 300 kV and liquid nitrogen temperature. The images were recorded in EFTEM mode using AFIS on K3 direct electron detector (Gatan, Inc.) and data acquisition software EPU (Thermo Fisher Scientific, Inc.). Exposures were for 1 s and were collected as 40-frame movies using total electron fluency (dose) of 49.75 $e^{-}/Å^2$ and defocus values between -2.4 and -1.0 µm. The movies were collected in super-resolution mode with nominal pixel size 0.415 Å, but were binned 2× following exposure, yielding effective pixel size of 0.83 Å/px.

MacAB-TolC-YbjP cryo-EM data processing

The cryo-EM data were processed using cryoSPARC 4.5 software (Structura Biotechnology, Inc.). Patch motion correction was used to correct for beam-induced motion and Patch CTF used to calculate the CTF. Circular Gaussian blob picking with a min/max diameter of 120/380 Å was used to extract an initial set of pixels in 878-px boxes Fourier-cropped to 600-px (effective pixel size 1.21 Å/px). After 2D classification these were used as input to a template-

picking model and particles re-extracted at 600-px and Fourier-cropped to 400-px (effective pixel size 1.245 Å/px). This set of particles was pruned again with another round of 2D classification and then subject to *ab-initio* reconstruction. The best volume and particles from 2D classification was used for heterogeneous refinement along with 5 'junk' volumes. The best output was then subjected to non-uniform refinement in C_1 symmetry with optimize per-particle defocus, optimize per-group CTF parameters, and fit spherical aberration options used to further improve the refinement. This yielded a 2.74 Å map with 233,835 particles. Finally, local CTF refinement, global CTF refinement, and another round of non-uniform refinement in C_1 was performed followed by reference-based motion correction. The unbinned output particles (233,775 particles at 600-px box size, 0.83 Å/px) were subjected to a final round of non-uniform refinement in C_3 symmetry yielding a final map with a GSFSC reported resolution of 2.48 Å. To facilitate model-building, DeepEMhancer was also run on this map. Data collection and processing parameters are shown in Table S1.

MacAB-TolC-YbjP model building and refinement

The part of the experimental map containing an unidentified protein density adjacent to TolC trimer was visualised and traced as a poly-alanine chain using Coot 0.9 (Emsley et al., 2010). The resulting structure model was submitted to the DALI server (Holm et al., 2023) to query the *E. coli* species subset of the AlphaFold Database (Hierarchical AF-DB Search). The search showed strong structural homology with the uncharacterised lipoprotein YbjP (AF-P75818-F1). The AlphaFold model was fitted into the experimental map and manually adjusted in Coot 0.9, allowing the identification of the density as YbjP. Following minor structure adjustments, the model was refined using ISOLDE 1.6 plugin (Croll 2018) for ChimeraX-1.6.1 (Pettersen et al., 2021). Molecular refinement was completed in Phenix-1.20 (Liebschner et al., 2019). Refinement statistics are listed in Table S1.

Preparation of AcrABZ-TolC in peptidisc reconstituted with YbjP

Co-expression of the recombinant AcrABZ-TolC-3xFLAG and cellular membrane preparation was as previously described with some modifications (Du et al., 2014). The AcrABZ-TolC-3xFLAG components were expressed into *E. coli* strain C43 (Δ*acrAB* and Δ*tolC*). Cell pellets were resuspended in lysis buffer (150 mM NaCl and 50 mM Tris pH 7.5) and membranes pelleted as previously described (Du et al., 2014) and solubilized with a buffer containing 400 mM NaCl, 50 mM Tris pH 7.5 and 1.5% (wt/v) β-DDM by stirring overnight at 4°C. The soluble extract was incubated with Ni-NTA beads (Qiagen) for nickel affinity purification (2

mL for 4.5 g membrane extract) of the histidine tagged $AcrABZ_{6xHis}$-$TolC_{3xFLAG}$. The beads were loaded onto a gravity flow-column and the column washed with 4 column volumes (CVs) of a buffer composed of 200 mM NaCl, 50 mM Tris pH 7.5 and 0.02% (wt/v) β-DDM. The $AcrABZ_{6xHis}$-$TolC_{3xFLAG}$ protein complex was eluted with the same buffer containing 0.5 M imidazole. Eluted fractions were analyzed on a 4-12% SDS-PAGE gel and fractions enriched for the pump were then pooled for a second purification step using anti-FLAG M2 affinity beads (Sigma). The fractions were incubated with 0.5 mL anti-FLAG resin for 3 hours at 4°C with gentle stirring and the beads were then washed with 2 CVs of buffer (200 mM NaCl, 50 mM Tris pH 7.5 and 0.02% β-DDM) and 3 CVs of buffer 200 mM NaCl, 50 mM Tris pH 7.5 to gradually decrease the detergent of the solubilized pump to below the critical micelle concentration. For reconstitution of the AcrABZ-TolC sample, the NSPr peptidisc was used based on the protocol by Carlson et al. (2018) with some modifications. Next, 2 mg mL^{-1} of peptidisc (Peptidisc Biotech) in 20 mM Tris-HCl pH 8.0 peptide solution was loaded to the column and incubated for 20 minutes at room temperature with gentle shaking. The flow-through was collected by gravity and 2 mg mL^{-1} peptide solution containing 40 µL of *E. coli* lipids (6 mg mL^{-1}) was loaded to the column and incubated with the beads. Finally, 0.5 mg mL^{-1} of 3xFLAG peptide in buffer 200 mM NaCl, 50 mM Tris pH 7.5 was added to the column and incubated with the beads for 15 minutes. The fractions were analyzed on a 4-12% gradient SDS-PAGE gel and concentrated to 5-6 mg mL^{-1} using a Vivaspin column with a 100 kDa MWCO.

Preparation of AcrABZ-TolC in peptidoglycan reconstituted with YbjP

AcrABZ-TolC-YbjP prepared with peptidoglycan extracts from *E. coli* several rounds of 2D classification were used to remove aberrant particles and the final particles were subjected in three state classification using *ab initio* reconstruction. Following several rounds of 3D homogeneous and non-uniform refinement a map was generated at 3.45 Å without application of symmetry restraints (C1) resolving the AcrABZ-TolC-YbjP but not the peptidoglycan layer along with an intermediate resolution map of the pump and likely the peptidoglycan indicating conformational heterogeneity in the dataset. For this, a tailored approach was taken to increase the content of the AcrABZ-TolC-YbjP peptidoglycan particle subset. 3D variability analysis (Punjani et al., 2017) was used as an alternative to 3D classification to identify distinct states. A consensus map was generated that includes both the particles and their respective alignments utilized for the reconstruction process.

AcrABZ-TolC-YbjP preparation with mature peptidoglycan and cryo-EM processing

The AcrABZ-TolC-YbjP was prepared in peptidisc following the procedure described for MacAB-TolC-YbjP with some modifications. The column was washed and eluted with buffer 50 mM Tris pH 7.5, 200 mM NaCl. Cryo-EM data processing and 3D-reconstructions were carried out using cryoSPARC (Punjani et al., 2017). Multiple rounds of 3D refinement were conducted including heterogeneous refinement to remove non-pump particles, along with homogeneous refinement and non-uniform refinement to improve the resolution. Samples of mature and early forms of peptidoglycan were kindly provided by Professor Waldemar Vollmer (University of Newcastle and now at University of Queensland, Brisbane, Australia), prepared from strains BW25113 ΔGLDT and C5703-1. His-tagged YbjP was prepared at 373 µM. Samples of AcrABZ-TolC in peptidisc were mixed with 10-fold excess YbjP and roughly 1 mg mL^{-1} of peptidoglycan slurry, incubated on ice for 1 hour and then used to prepare grids on glow-discharged Ultrafoil R 1.2/1.3 using a FEI Vitrobot (IV) at settings of 95% humidity, 4°C, 3 seconds blot time, -5 force. Through 3DVA (3-dimensional variability analysis), two main particle classes of AcrABZ-TolC-PG-YbjP and AcrABZ-TolC-YbjP were sub-classified enabling 3D reconstructions at 3.97 Å and 3.45 Å resolution, respectively. The data collection and processing parameters are summarised in Table S2.

Plasmid construction and purification of soluble YbjP

A soluble YbjP was constructed by amplifying the protein globular domain (residues 28-171) from *E. coli* MG1655 genomic DNA. The PCR product was digested NdeI-BamHI prior insertion into pET28a digested with the same enzymes. *E. coli* BL21 (DE3) cells were then transformed with pET28-$YbjP_s$ plasmid encoding a soluble YbjP bearing an N-terminal His-tag. Bacteria were grown at 37°C in 2YT media supplemented with kanamycin and protein expression induced with addition at mid- to late-log phase of 0.1 mM IPTG. After 16h at 18°C, cells were harvested by centrifugation (4,000 *g*, 10 min), and pellets resuspended in 50 mM Tris pH 7.5, 200 mM NaCl and 10% glycerol supplemented with lysozyme and DNase I. Cells were then lysed by passage through a cell disruptor (Constant Systems) at 30,200 psi. Unbroken cells and debris were removed by ultracentrifugation (1h, 107,000 *g*, 4°C). The supernatant was supplemented with 20 mM imidazole and loaded onto a 5 mL HisTrap FF column using an ÄKTAxpress FPLC (GE Healthcare). The column was washed with 15 column volumes of the same buffer before elution with 250 mM imidazole. Protein fractions were pooled, dialysed twice against 2L of buffer containing 50 mM Tris pH 7.5 and 200 mM NaCl and concentrated using a Vivaspin column with a 10 kDa MWCO before flash freezing and storage at -80°C.

Isothermal titration calorimetry (ITC)

Experiments were performed with a ITC200 calorimeter (MicroCal, Malvern Panalytical) at 25°C. After overnight dialysis in 20 mM Hepes pH 7.5, 200 mM NaCl, 0.03% (wt/v) DDM, soluble, N-terminally his-tagged YbjP (residues 28 to 171) at 230 µM was injected into 40 µM TolC in the same buffer. The titration program consisted of 25 injections of 1.5 µL with an initial injection of 0.4 µL every 300 s, with cell stirring rate of 750 rpm. For each condition, a control titration was performed by injecting YbjP into a cell containing buffer only. The control signal was then subtracted from the experimental titration, and the binding affinity, stoichiometry and thermodynamic parameters were obtained by nonlinear least-squares fitting of the background corrected experimental data using a single-site binding model from the MicroCal PEAQ-ITC analysis software (Malvern). ITC parameters are listed in Table S3.

IMAC (immobilised metal affinity chromatography) binding assay of TolC and YbjP

Detergent-purified Flag-tagged TolC was mixed to soluble YbjP bearing a N-terminal His-tag for 5 minutes in 50 mM Tris pH 7.5, 200 mM NaCl and 0.03% (wt/v) β-DDM. Each protein was at 15 µM final concentration in a final volume of 125 µL. A control was realized with only the TolC protein, or only the YbjP, or by replacing YbjP with another periplasmic protein, soluble LolB, produced as described in (Kaplan et al. 2018). Proteins were added to 100 µL of Ni-resin (50% slurry, profinity Biorad) in a microbatch spin column and after 5 minutes the flow-through was recovered. The resin was washed four times with 250 µL of buffer and bound proteins were eluted with the same volume of buffer containing 250 mM imidazole. Elution fractions were analyzed on a gradient (4-12%) SDS-PAGE gel. As a reference the TolC flow-through fraction was also loaded.

In vivo photo-crosslinking

Plasmid constructions. Full-length YbjP was amplified from *E. coli* MG1655 genomic DNA. A Ser-Gly linker followed by a hexaHistidine tag was added on the reverse primer. The PCR product was digested by NdeI-Xho and inserted into pET24a digested by the same enzymes. AcrA was cloned as described for YbjP. Amber codons were introduced at desired positions by Quikchange site-directed mutagenesis.

Culture and photo-crosslinking. E. coli C43 cells were co-transformed with pEVOL encoding an amber suppressor tyrosyl tRNA and the engineered tyrosyl tRNA synthetase (Chatterjee et

al., 2014) and with pET-24 bearing full-length C-terminally His-tagged YbjP or AcrA amber mutant for incorporation of pBPA into the TAG amber codon at desired positions. Cultures of 20 mL LB media, supplemented with 20 and 50 µg mL^{-1} of chloramphenicol and kanamycin A respectively, were inoculated with 1/100 of overnight cultures and grown at 30°C. When an optical density of 0.3 was reached, 1 mM of freshly prepared pBPA (Bachem) in NaOH was added in each culture with additional HCl to balance pH. When indicated, a control without addition of pBPA was realised. After 30 min at 30°C, cells were induced with 0.02% (wt/v) L-arabinose and 0.5 mM IPTG and grown for 2h at 30°C. Cells corresponding to 4 mL of culture were collected by centrifugation (4,000 *g*, 4°C, 4 minutes) washed with 1 mL of PBS and resuspended in 700 µL PBS. Aliquots of 150 µL of each culture were transferred in a 96-well plate and exposed under UV (365 nm) for 15 min at room temperature using a UVGL-58 handheld UV lamp.

His-tag enrichment. The next day, samples were lysed by 3 cycles of freezing in liquid nitrogen and thawing in 37°C water bath. Lysozyme at 0.5 mg mL^{-1}, DNase at 50 µg mL^{-1} and 1% (wt/v) DDM were added. After 30 min at room temperature, samples (300 µL) were transferred into spin columns containing 100 µL of Ni-NTA resin (50% suspension, profinity Biorad) previously equilibrated with PBS (phosphate buffered saline). Proteins were allowed to bind for 5 min at room temperature. The resin was then washed 3 times with 400 µL of PBS supplemented with 0.03% DDM and bound proteins eluted with 150 µL of PBS containing 0.03% DDM and 250 µM imidazole.

Western-blot. Samples (20 µL) were analyzed by SDS-PAGE and immunoblotting with anti-histidine primary antibodies (Penta-His, Qiagen) and goat anti-mouse secondary antibodies (IRDye 800 CW, Licor) prior to imaging with an Odyssey Licor system.

Agar-plate and liquid growth assays

E. coli K12 BW25113 WT or Δ*ybjp* (JW0849) from the Keio collection were grown at 37°C in LB media in the presence or absence of benzalkonium chloride (BZK) at 10 µg mL^{-1}. Growth was followed by measuring the optical density at 600 nm every 20 minutes for 200 minutes, and then every 40 minutes.

YbjP cellular localization and immunoblotting

Starter cultures of BW25113 (WT) and JW0849 (Δ*ybjP*) *E. coli* strains from the Keio collection

were grown overnight in 2YT media at 37°C and used to inoculate containing 1 L-flasks the next day. At OD_{600nm} of 0.1-0.2, chloramphenicol at 2 µg mL^{-1} final concentration was added in half of the conditions and cells cultured until they reached an OD_{600nm} of 0.5-0.6. Bacteria were collected by centrifugation (4,000 *g*, 30 min, 4°C) and pellets resuspended in 30 mL of a buffer containing 50 mM Tris-HCl pH 8.0. Bacteria suspensions were divided in two halves and the 15 mL were centrifuged (4,000 *g*, 20 min, 4°C). One of the pellets was kept for membrane extraction and the other was used to extract periplasm fractions by cold osmotic shock in the presence of EDTA and lysozyme.

For periplasm extraction, cells were converted into spheroplasts by resuspending the pellet in 40 mL of buffer (50 mM Tris-HCl pH 8.0, 6 mM EDTA and 500 mM sucrose) with an EDTA-free protease inhibitor mixture tablet (Roche) and 5 mg mL^{-1} lysozyme. After 40 min of incubation at 4°C, 20 mM $MgCl_2$ and 400 U of DNase I were added. Solutions were incubated for 30 min at 4°C prior to pellet the spheroplasts and intact cells by centrifugation (12,000 *g*, 20 min, 4°C). The outer membranes present in the supernatant were removed by centrifugation (145,000 *g*, 3 h, 4°C) and the periplasmic fractions (supernatant) analyzed by SDS-PAGE.

For membrane extraction, cells were resuspended in 40 mL of a buffer (20 mM Tris-HCl pH 8.0, 400 mM NaCl) with an EDTA-free protease inhibitor mixture tablet, lysozyme and DNase I as for periplasm extraction. After 1h incubation at 4°C, bacteria suspensions were passed twice through a Cell disruptor (Constant Systems) at 30,000 psi at 4°C. Lysates were centrifuged at 9,000 *g* for 30 min at 4°C to remove the cell debris, and the membranes were collected by centrifugation (145,000 g, 3h, 4°C). Outer and inner membranes were separated on a sucrose gradient (12 mL at 73%, 12 mL at 53% and 9 mL at 20%). Total membranes were resuspended in 2 mL of a buffer containing 50 mM Tris-HCl pH 8.0, 20% sucrose and 1 mL of the solution was overlaid on the top of the sucrose gradient prior centrifugation (145,000 *g*, 18h, 4°C without braking). Two nicely separated bands were observed after centrifugation. The upper band layer (inner membrane) was collected using a fine pipette and, to avoid mixing the fractions, the lower band (outer membrane) was obtained by piercing the bottom of the tube. The periplasmic, inner membrane and outer membrane fractions were analyzed by SDS-PAGE and immunoblotting with anti-TolC primary antibodies and donkey anti-rabbit secondary antibodies (IRDye 680 RD, Licor) prior to imaging with an Odyssey Licor system.

Phylogenetic analysis of DUF3828 domain

3327 proteins containing DUF3828 domain (PF12883) were acquired from InterPro (v103), and the domain architectures represented by *E. coli* YbjP and YqhG were selected. Taxonomy information was retrieved from UniProt on Dec 22, 2024, and the signal peptide was predicted by SignalP 6.0 (Teufel *et al*., 2022). After removing proteins with unidentified taxonomy, representative sequences were selected by manual inspection of *E. coli* and *Salmonella* and CD-HIT with a 95% identity threshold (Fu *et al*., 2012), yielding 356 sequences. The multiple sequence alignment was generated by hmmalign using the PF12883 HMM profile and processed with TrimAl on automated mode (Capella-Gutiérrez *et al*., 2009). A phylogenetic tree was constructed from the resulting multiple sequence alignment using IQ-Tree2 on a default parameter (Nguyen *et al*., 2015). The tree was rooted using the minimal ancestor deviation method (Tria *et al*., 2017), yielding the same result. Annotation was performed with TreeViewer (Bianchini & Sánchez-Baracaldo, 2024) and webFlaGs (Saha *et al*., 2021) was used to analyze the gene synteny of DUF3828-containing proteins.

Bioinformatic analysis of outer membrane efflux protein

Outer membrane efflux proteins (IPR003423) and TolC proteins (IPR010130) were acquired from InterPro (v103) and the taxonomic information was retrieved from UniProt on Dec 22 2024. The signal peptide was predicted by SignalP6.0. Outer membrane efflux proteins of *Pseudomonadota* were selected and clustered with CLANS (CLuster ANalysis of Sequences) (Frickey and Lupas, 2004).

For the phylogenetic analysis of TolC, the method described for DUF3828 analysis was used with some modifications. Sequences of *Pseudomonadota* were collected, and the sequence showing the highest sequence similarity to *E. coli* TolC in each organism was selected. Redundant sequences were removed by CD-HIT with a 90% identity threshold. In addition, a phylogenetic tree was constructed using FastTree on -mlacc 2 -slowni parameter (Price *et al*., 2010).

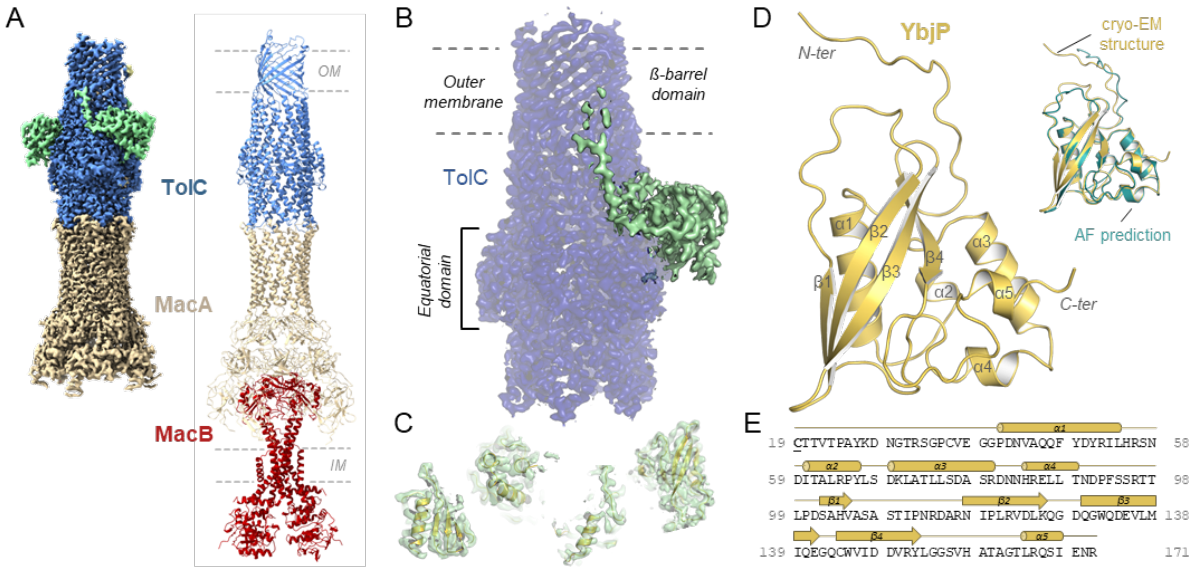

Figure 1. TolC partner identified by cryo-EM. (A) Cryo-EM density map (*left*) and model (*right)* for the tripartite pump MacA-MacB-TolC (PDB 5NIL). Density for the MacB dimer is less well defined. (B) Close-up view on the TolC region showing additional density in *green*. TolC domain organisation is indicated. (C) Modelling of secondary structural elements fitting in the additional density. (D) The refined structure of the TolC partner, YbjP. After lipoprotein maturation, the N-terminal cysteine carries a lipid modification which is not shown here. Alignment of the YbjP structure from cryo-EM and corresponding AlphaFold prediction model is shown as *inset*. (E) Sequence and secondary structure alignment annotation of mature YbjP. The tri-acylated cysteine (C19) conserved in lipoproteins is underlined.

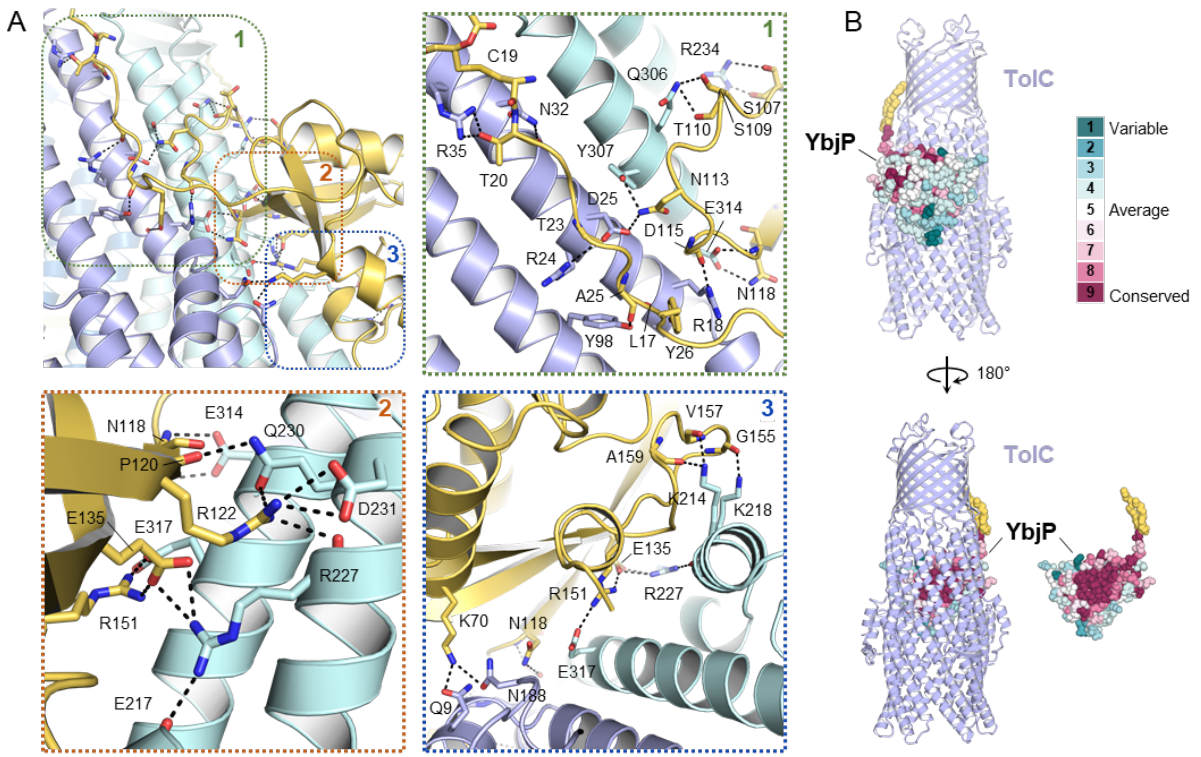

Figure 2. Interactions in the TolC-YbjP complex. (A) Overview of protein-protein interactions with close-up views presented in panels 1, 2 and 3. The YbjP lipoprotein (*yellow*) contacts two adjacent protomers of the TolC trimer (*blue*). Lipoprotein acyl modification and residues involved in intermolecular contacts are shown in stick representation. (B) Residue variability analysis of YbjP highlighting the clustering of conserved residues at the TolC interface. Analysis was performed with the CONSURF server. YbjP is shown as spheres with the lipoylation in *yellow*.

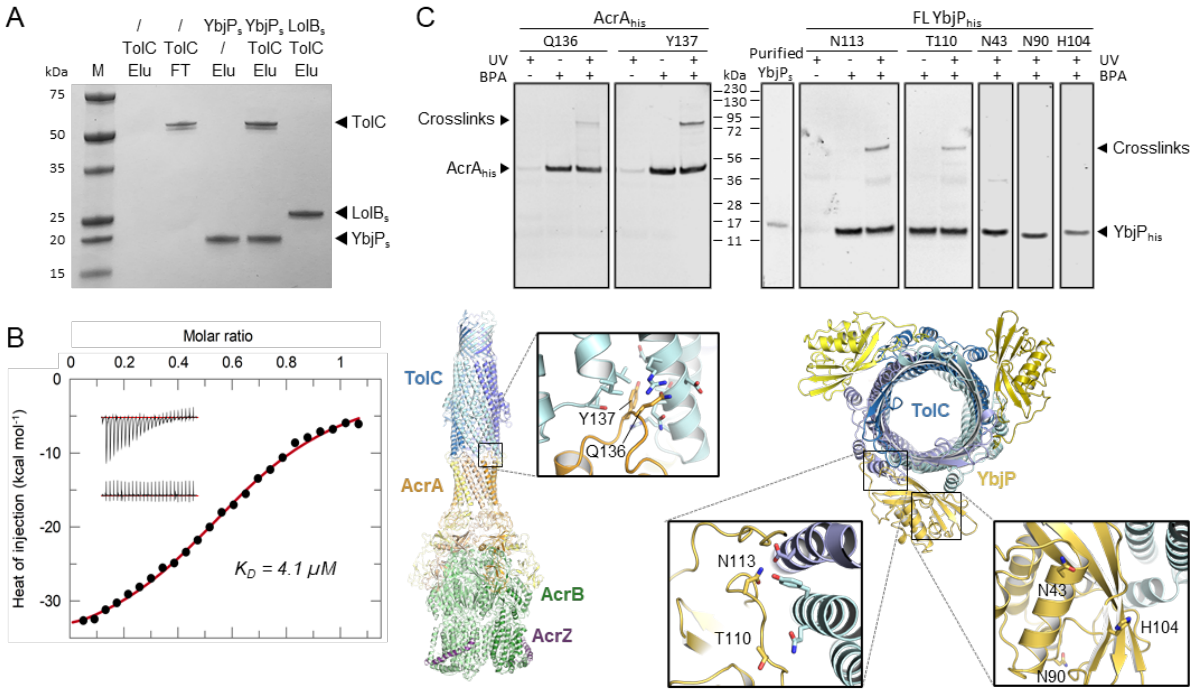

Figure 3. *In vitro* and *in vivo* experiments probing the TolC-YbjP interface. (A) *In vitro* binding assay between TolC and soluble YbjP ($YbjP_s$) that is missing the lipid modification. TolC-flag was mixed with histidine-tagged $YbjP_s$ or soluble LolB ($LolB_s$) prior immobilization on IMAC resin. After several washes, the elution fractions (Elu) were analyzed by SDS-PAGE. Molecular masses of protein standards (M) are indicated. (B) Isothermal titration calorimetry (ITC) profile for the interaction of TolC and $YbjP_s$. Background-corrected heats of injection are shown together with a fitted binding curve in *red*. The raw thermograms corresponding to the injection of $YbjP_s$ into a TolC-containing cell or into buffer are shown in *upper* and *lower inlets*, respectively. ITC parameters are listed in Table S3. (C) *In vivo* validation of the interaction between full-length (FL) YbjP and TolC by photo-crosslinking. The experimental procedure was validated using another periplasmic lipoprotein, AcrA, which associates with TolC. In brief, *E. coli* C43 cells expressing $YbjP_{his}$ or $AcrA_{his}$ mutants carrying a photoactivatable pBPA group at indicated positions were grown in the presence (+) or absence (-) of pBPA and irradiated (+) or not (-) with UV. Cells were then lysed by successive freeze-thaw cycles, solubilized with DDM and lysates purified by Ni-NTA chromatography. Eluted proteins were analyzed by SDS-PAGE and immunoblotting using anti-his antibodies. Purified $YbjP_s$ protein was also loaded as a benchmark control. Presence of crosslinked products are indicated with a black arrow. The expected sizes of proteins are as follows: AcrA, 40 kDa; YbjP, 17 kDa; and TolC, 54 kDa.

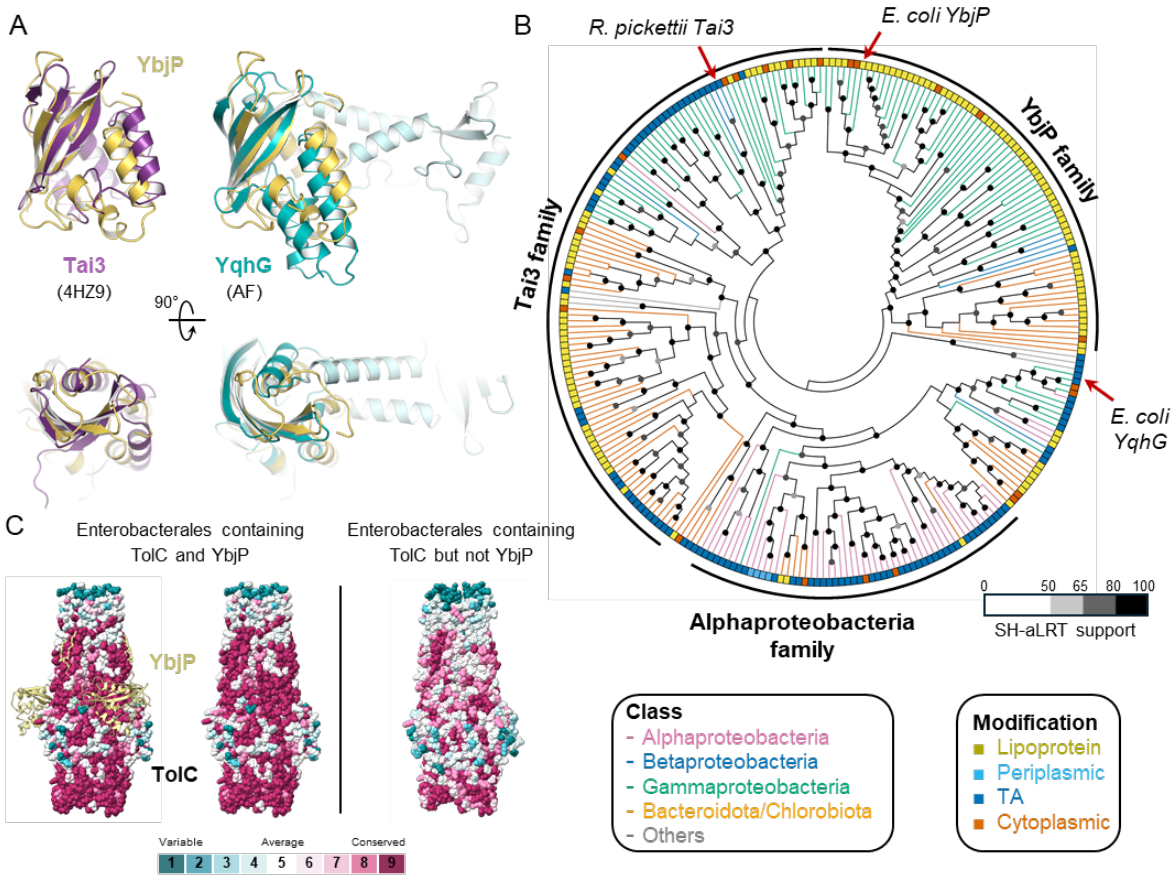

Figure 4. Analysis of YbjP evolution and co-evolution with TolC. (A) Structural alignment of YbjP with other DUF3828-containing proteins: Tai3 (4HZ9, purple) and YqhG (AlphaFold Q46858, blue). A 90° rotation along the *x*-axis is shown underneath. (B) A cladogram of DUF3828-containing proteins. The reviewed proteins (Tai3, YbjP and YqhG) are marked by an arrow. (C) Surface conservation of TolC proteins from Enterobacterales containing or not YbjP. Results are displayed on *E. coli* TolC on the *left* and on *P. atrosepticum* TolC (AlphaFold model, Q6DAC5) on the *right*. For clarity, YbjP is displayed on the *left* panel but not on the *right*. Analysis was performed with the CONSURF server.

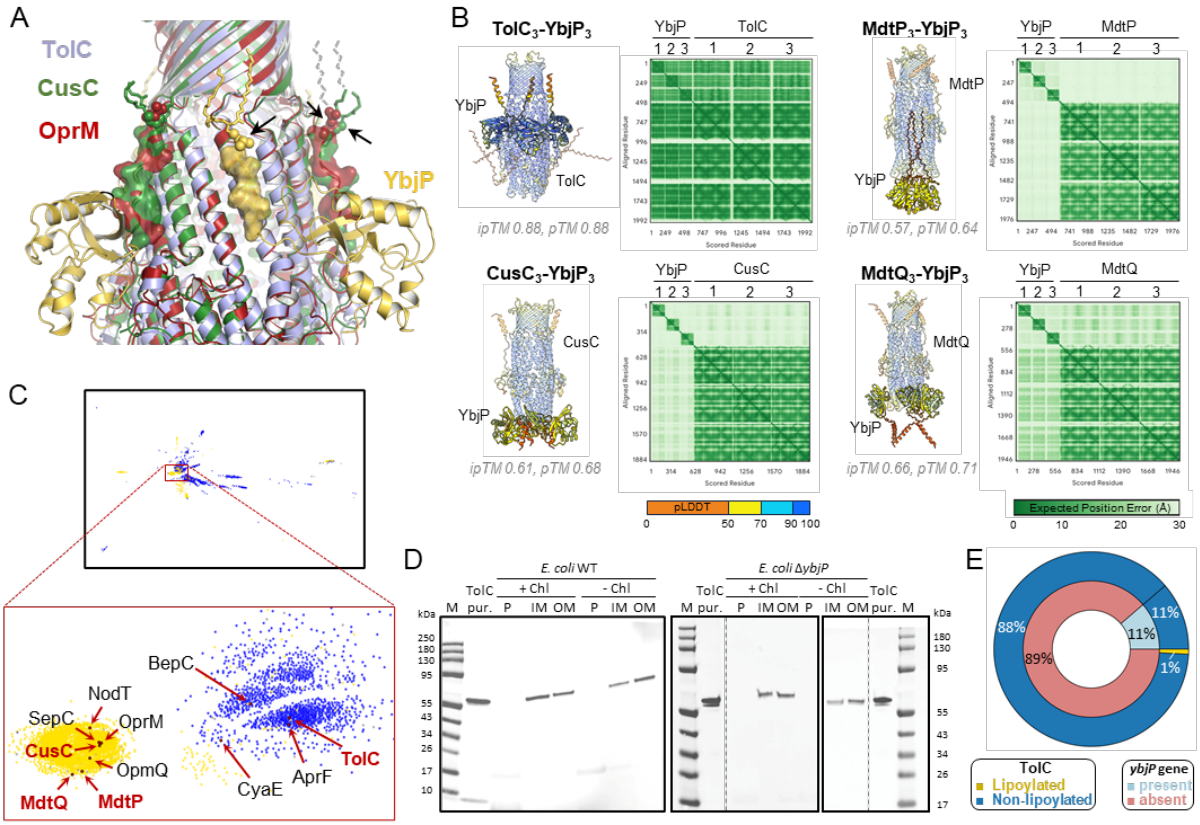

Figure 5. YbjP lipoprotein is not required for TolC trafficking in *E. coli*. (A) Structural alignment of *E. coli* TolC (*blue*), CusC (3PIK, *green*) and *P. aeruginosa* OprM (3D5K, *red*). The YbjP or TolC-homologue linker is shown as transparent surface and modified cysteines are indicated by an arrow. Dashes lines show the extension of the lipid group (partially- or non-modelled in the structures). (B) AlphaFold3 prediction (Abramson *et al*., 2024) between *E. coli* outer membrane efflux proteins and YbjP. The model with the higher ipTM and pTM scores is shown out of three technical repeats. (B) CLANS analysis of outer membrane efflux proteins (IPR003423) in *Pseudomonadota*. Clustering was performed in 2D until equilibrium. Outer membrane proteins in *E. coli* are shown in *red*, and other key reviewed proteins in *black*. *Yellow*, lipoylation; *blue*, secreted; *grey*, other. (D) Immunoblot showing the localization of TolC in *E. coli* wild-type or Δ*ybjP* cultured (+) or not in the presence of chloramphenicol (Chl). Cells were lysed and membranes separated on a sucrose gradient. Periplasmic fractions were obtained from spheroplast preparation as described in the Methods. Samples corresponding to the periplasmic fraction (P), the inner (IM) or the outer (OM) membranes were subjected to immunoblotting using anti-TolC antibodies. Purified (pur.) TolC protein served as control for the antisera. (E) Distribution of the *ybjP* gene and lipoylated TolC in Gammaproteobacteria. Repartitions are as follows: *ybjP* present (*light blue*, n=67) or absent (*magenta*, n=525); lipoylated (*yellow*, n=5) or non-lipoylated TolC (*dark blue*, n=587).

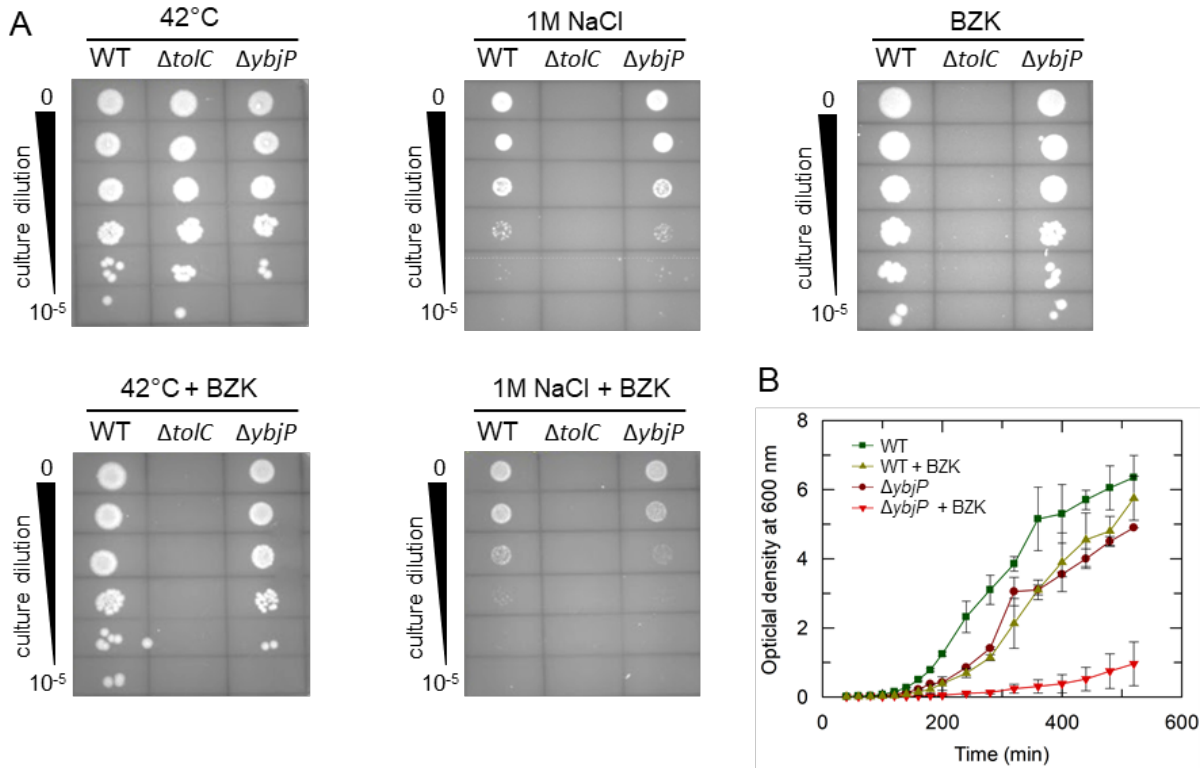

Figure 6. Impact of YbjP on *E. coli* growth under stress conditions. (A) Dilution series on nutrient agar plates at 42ºC temperature (*left*), in the presence of high salt concentration (1M NaCl, *middle*) or sublethal amounts of benzalkonium chloride (BZK, 10 µg mL^{-1}, *right*). Plates combining grown at 42ºC (*left*) or with 1M NaCl (*right*) and presence of BZK at the same concentration are displayed underneath. (B) Growth curves of WT and YbjP null strains in the absence or presence of 10 µg mL^{-1} benzalkonium chloride. Curves depict the mean ± standard deviation for two independent cultures.

Data availability

The MacAB-TolC-YbjP atomic model and electron microscopy maps have been deposited in the Protein Data Bank (PDB) and Electron Microscopy Data Bank (EMDB) under the accession codes 9QGY and EMDB-53150 respectively.

Acknowledgements

JG was supported by an Amgen scholarship. Grids were prepared and cryo-EM data collected at the BIOCEM facility, Department of Biochemistry, University of Cambridge. We thank Dimitri Y. Chirgadze, Steven Hardwick, and Lee Cooper for assistance with data collection and

processing at the Cryo-EM Facility. We thank Liz Sockett and Waldemar Voller for helpful discussions, and Waldemar for providing mature and early forms of peptidoglycan.

Funding

This work is supported by an ERC Advanced Award and Wellcome Trust Investigator Awards (222451/Z/21/Z and 200873/Z/16/Z).

Conflicts of Interest

The authors declare no conflict of interest.

REFERENCES

Aicart-Ramos C, Valero RA, Rodriguez-Crespo I. (2011) Protein palmitoylation and sub cellular trafficking. *Biochim Biophys Acta* 1808, 2981-2994.

Babu M, Bundalovic-Torma C, Calmettes C, Phanse S, Zhang Q, Jiang Y, Minic Z, Kim S, Mehla J, Gagarinova A, Rodionova I, Kumar A, Guo H, Kagan O, Pogoutse O, Aoki H, Deineko V, Caufield JH, Holtzapple E, Zhang Z, Vastermark A, Pandya Y, Lai CC, El Bakkouri M, Hooda Y, Shah M, Burnside D, Hooshyar M, Vlasblom J, Rajagopala SV et al. (2017) Global landscape of cell envelope protein complexes in *Escherichia coli. Nat. Biotechnol.* Pubmed:29176613

Bergès, C. et al. (2021) Exploring the glucose fluxotype of the E. coli y-ome using high-resolution fluxomics. *Metabolites* 11(5). doi: 10.3390/metabo11050271.

Calladine, C.R., Sharff, A. & Luisi, B. (2001) How to untwist an alpha-helix: structural principles of an alpha-helical barrel. *J. Mol. Biol.* 305, 603-618.

Carlson ML, Young JW, Zhao Z, Fabre L, Jun D, Li J, Li J, Dhupar HS, Wason I, Mills AT, Beatty JT, Klassen JS, Rouiller I & Duong F (2018) The peptidisc, a simple method for stabilizing membrane proteins in detergent-free solution. *Elife* 7: 1–23.

Chatterjee D, Cooley RB, Boyd CD, Mehl RA, O'Toole GA, Sondermann H. (2014) Mechanistic insight into the conserved allosteric regulation of periplasmic proteolysis by the signaling molecule cyclic-di-GMP. *Elife* 3: e03650. https://doi.org/10.7554/eLife.03650.

Croll TI (2018) ISOLDE: a physically realistic environment for model building into low-resolution electron-density maps. *Acta Crystallogr D Struct Biol* 74, 519-530.

Du, D, Wang-Kan, X., Neuberger, A., van Veen HW, Pos, K.M., Piddock. LJV, and Luisi, B.F. (2018) Multidrug efflux pumps: structure, function and regulation. *Nat Rev Microbiol.* 16:523-539. doi: 10.1038/s41579-018-0048-6.

Fitzpatrick, A.W.P., Llabres, S., Neuberger, A., Blaza, J.N., Bai, X-C, Okada, U., Murakami,

S., van Veen, H.W., Zachariae, U., Scheres, S.H.W, Luisi, B.F. and Du, D. (2017) Structure of the MacAB-TolC ABC-type tripartite multidrug efflux pump. *Nature Microbiology* 2:17070.

Franklin, M.W., Nepomnyachiy, S., Feehan, R., Ben-Tal, N., Kolodny, R. and Slusky, J.S.G. (2018) Efflux pumps represent possible evolutionary convergence onto the beta-barrel fold. *Structure* 26, 1266-1274.

Glavier M, Puvanendran D, Salvador D, Decossas M, Phan G, Garnier C, et al. (2020) Antibiotic export by MexB multidrug efflux transporter is allosterically controlled by a MexA-OprM chaperone-like complex. *Nat Commun.* 11(1):4948. https://doi.org/10.1038/s41467-020-18770-5 PMID: 33009415; PubMed Central PMCID: PMC7532149.

Guest, RL & Silhavy, TJ (2023) Cracking outer membrane biogenesis. *BBA Mol Cel Res* 1870, 119405.l

Gumbart, J. C., Ferreira, J. L., Hwang, H., Hazel, A. J., Cooper, C. J., Parks, J. M., Smith, J. C., Zgurskaya, H. I., & Beeby, M. (2021). Lpp positions peptidoglycan at the AcrA-TolC interface in the AcrAB-TolC multidrug efflux pump. *Biophysical Journal*, 120(18), 3973–3982.

Hoang HH, Nickerson NN, Lee VT, Kazimirova A, Chami M, Pugsley AP, et al. (2011) Outer membrane target- ing of Pseudomonas aeruginosa proteins shows variable dependence on the components of Bam andLol machineries. *mBio*. 2(6). https://doi.org/10.1128/mBio.00246-11 PMID: 22147293; PubMed Central PMCID: PMC3230066.

Holm, L. (2022). Dali server: structural unification of protein families. *Nucleic Acids Research*, *50*(W1), W210–W215. https://doi.org/10.1093/nar/gkac387

Honeycutt, J.D., Wenner, N., Li, Y., Brewer, S.M., Massis, L.M., Brubaker, S.W., Chairatana, P., Owen, S.V., Canals, R., Hinton, J.C.D., Monack, D.M. (2020) Genetic variation in the MacAB-TolC efflux pump influences pathogenesis of invasive Salmonella isolates from Africa. *PLoS Pathog* 16(8): e1008763.

Horne, J.E., Brockwell, D.J. and Radford, S.E. (2020) Role of the lipid bilayer in outer membrane protein folding in Gram-negative bacteria. *J. Biol. Chem*. 295, 10340-10367.

Huang, P.-S., Oberdorfer, G., Xu, C., Pei, X.Y., Nannenga, B.L., Rogers, J.M., DiMaio, F., Gonen, T., Luisi, B.F. and Baker, D. (2014) High thermodynamic stability of parametrically designed helical bundles. Science 346, 481-485. Doi; 10.1126/science.1257481. PMID: 25342806

Jumper, J., Evans, R., Pritzel, A., Green, T., Figurnov, M., Ronneberger, O., Tunyasuvunakool, K., Bates, R., Žídek, A., Potapenko, A., Bridgland, A., Meyer, C., Kohl, S. A. A., Ballard, A. J., Cowie, A., Romera-Paredes, B., Nikolov, S., Jain, R., Adler, J., … Hassabis, D. (2021). Highly accurate protein structure prediction with AlphaFold. *Nature*, *596*(7873), 583–589. https://doi.org/10.1038/s41586-021-03819-2

Kaplan, E., Greene, N.P., Crow, A. And Koronakis, V. (2018) Insights into bacterial lipoprotein trafficking from a structure of LolA bound to the LolC periplasmic domain. Proc Natl. Acad Sci U.S.A. 115, E7389-7397.

Kovacs-Simon, A., Titball, R. W. and Michell, S. L. (2011) Lipoproteins of bacterial pathogens. *Infection and immunity*, 79(2), 548–561. doi: 10.1128/iai.00682-10.

Lei, H-T, Bolla, J.R., Bishop, N.R, Su, C-C, Yu, E.W. (2014) Crystal structures of CusC review conformational changes accompanying folding and transmembrane channel formation. *J. Mol. Biol.* 426, 403-411.

Liebschner et al. (2019) Macromolecular structure determination using X-rays, neutrons and electrons: recent developments in Phenix. *Acta Crystallography D Struct Biol* 75, 861-877.

Linder, M.E. and Deschenes, R.J. (2007) Palmitoylation: policing protein stability and traffic. *Nat Rev Mol Cell Biol* 8, 74-84.

Malinverni JC, Werner J, Kim S, Sklar JG, Kahne D, Misra R, et al. (2006) YfiO stabilizes the YaeT complex and is essential for outer membrane protein assembly in *Escherichia coli*. *Mol Microbiol.* 61 (1):151–64. https://doi.org/10.1111/j.1365-2958.2006.05211.x PMID: 16824102.

Miller, E.N. (2023) Elucidating the role of the membrane associated protein, YbjP, in *Klebsiella pneumonia*. MPhil thesis, University of Edinburgh.

Molloy, M.P., Herbert, B.R., Slade, M.B., Rabilloud, T., Nouwens, A.S., Williams, K.L., Gooley, A.A. (2000) Proteomic analysis of the *Escherichia coli* outer membrane. *Eur J. Biochem* **267**, 2871-2881.

Nakayama, H., Kurosawa, K. And Lee B.L. (2012). Lipoproteins in bacteria: structures and biosynthetic pathways. *FEBS J.* 279, 4247-4268.

Pattrick, C. A. et al. (2019) Proteomic profiling, transcription factor modeling, and genomics of evolved tolerant strains elucidate mechanisms of vanillin toxicity in *Escherichia coli*. *mSystems*, 4(4). doi: 10.1128/mSystems.00163-19.

Stubenrauch, C.J., Bamert, R.S., Wang, J., and Lithgow, T. (2022) A noncanonical chaperone interacts with drug efflux pumps during their assembly into bacterial outer membranes. *PLoS Biol*. 20: e3001523.

Tenorio, E., Saeki, T., Fujita, K., Kitakawa, M., Bab, T., Mori, H., Isono K. (2003) Systematic characterization of Escherichia coli genes/ORF affecting biofilm formation. *FEMS Microbiol Lett* 225, 107-114.

Tsutsumi K, Yonehara R, Ishizaka-Ikeda E, Miyazaki N, Maeda S, Iwasaki K, et al. (2019) Structures of the wild-type MexAB-OprM tripartite pump reveal its complex formation and drug efflux mechanism. *Nat Commun.* 10(1):1520. https://doi.org/10.1038/s41467-019-09463-9 PMID: 30944318; PubMed Central PMCID: PMC6447562.

Voulhoux, R., Bos, M. P., Geurtsen, J., Mols, M. & Tommassen, J. (2003) Role of a highly conserved bacterial protein in outer membrane protein assembly. *Science* 299, 262–265.

Wang Z, Fan G, Hryc CF, Blaza JN, Serysheva II, Schmid MF, et al. (2017) An allosteric transport mechanism for the AcrAB-TolC multidrug efflux pump. *eLife* 6. doi.org/10.7554/ eLife.24905 PMID: 28355133; PMC5404916.

Werner J, Misra R. (2005) YaeT (Omp85) affects the assembly of lipid-dependent and lipid-independent outer membrane proteins of *Escherichia coli*. *Mol Microbiol.* 57(5):1450–9. Epub 2005 Aug 17. https:// doi.org/10.1111/j.1365-2958.2005.04775.x PMID: 16102012.

Wu, T. et al. (2005) Identification of a multicomponent complex required for outer membrane biogenesis in *Escherichia coli*. *Cell* 121, 235–245.

Zhang, W., Harper, C.E., Lee, J., Fu, B., Ramsukh, M., Hernandez, C.J., Chen P. (2025) Transporter excess and clustering facilitate adaptor protein shuttling for bacterial efflux. *Cell Reports Physical Science* 6, 102441.

Supplementary Information For

A lipoprotein partner for the *Escherichia coli* outer membrane protein TolC

Jim Horne*, Elise Kaplan*[+], Ben HS Jin, Emmanouela Petsolari, Jan M. Gradon[++], Yvette Ntsogo, Andrzej Harris, Dingquan Yu, Ben F. Luisi

Department of Biochemistry, University of Cambridge, Tennis Court Road, Cambridge CB2 1GA, UK

[+]current address, Molecular Microbiology and Structural Biochemistry (MMSB), UMR 5086 CNRS/University of Lyon, Lyon, France

[++]current address, School of Biochemistry, Faculty of Life Sciences, University of Bristol, Bristol BS8 1TD, United Kingdom

*equal contributions

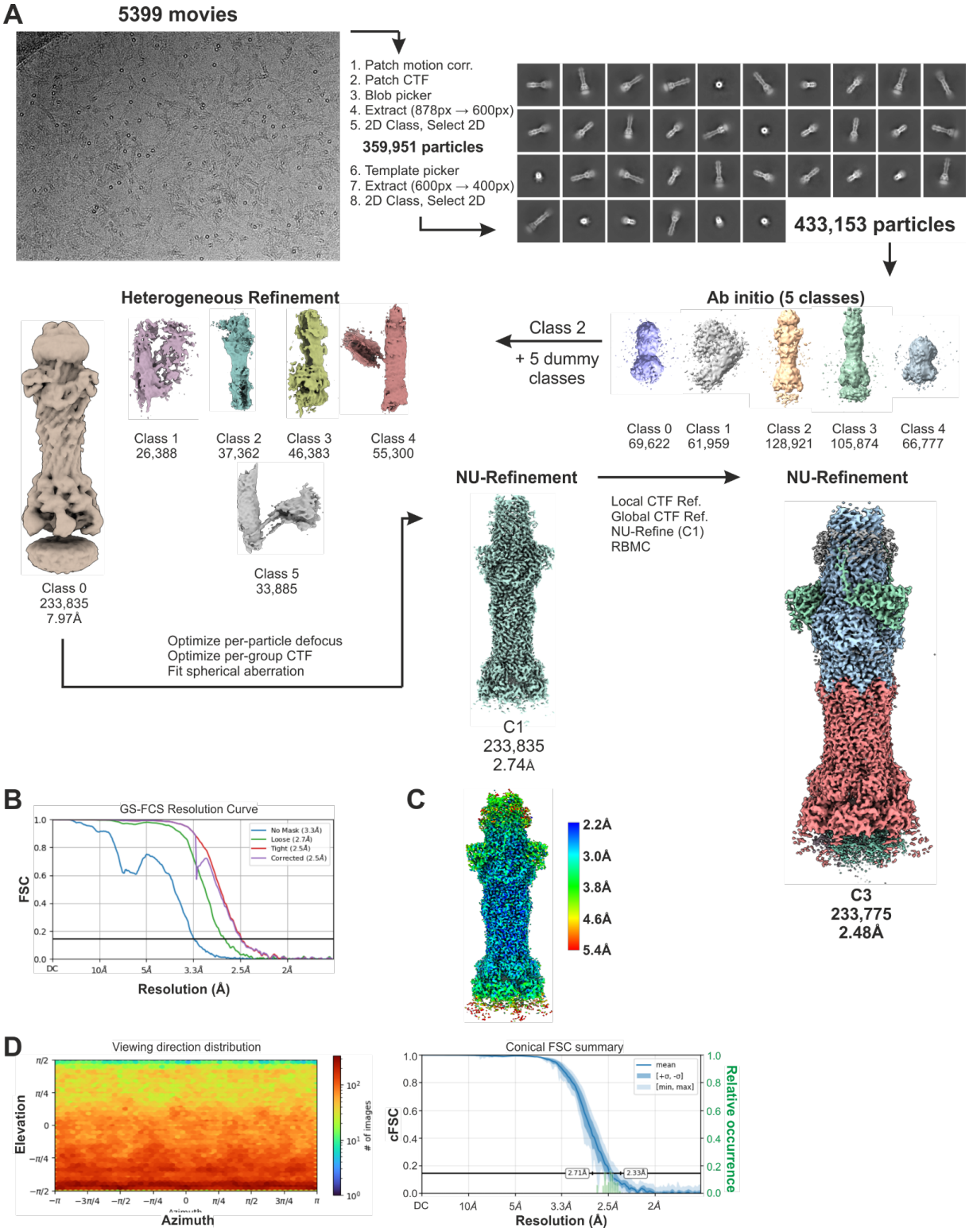

Supplementary Figure S1. Cryo-EM processing workflow for MacAB-TolC-YbjP complex. (A) Cryo-EM processing workflow. (B) Gold-standard Fourier Shell Correlation (GS-FSC) curves for final reconstruction. (C) Local resolution distribution in final map. (D) Angular distribution plot for final map, *left*, and Fourier Shell Correlation between half maps of MacAB-TolC-YbjP, *right*. These data suggest that there is not a large orientational bias in the final map.

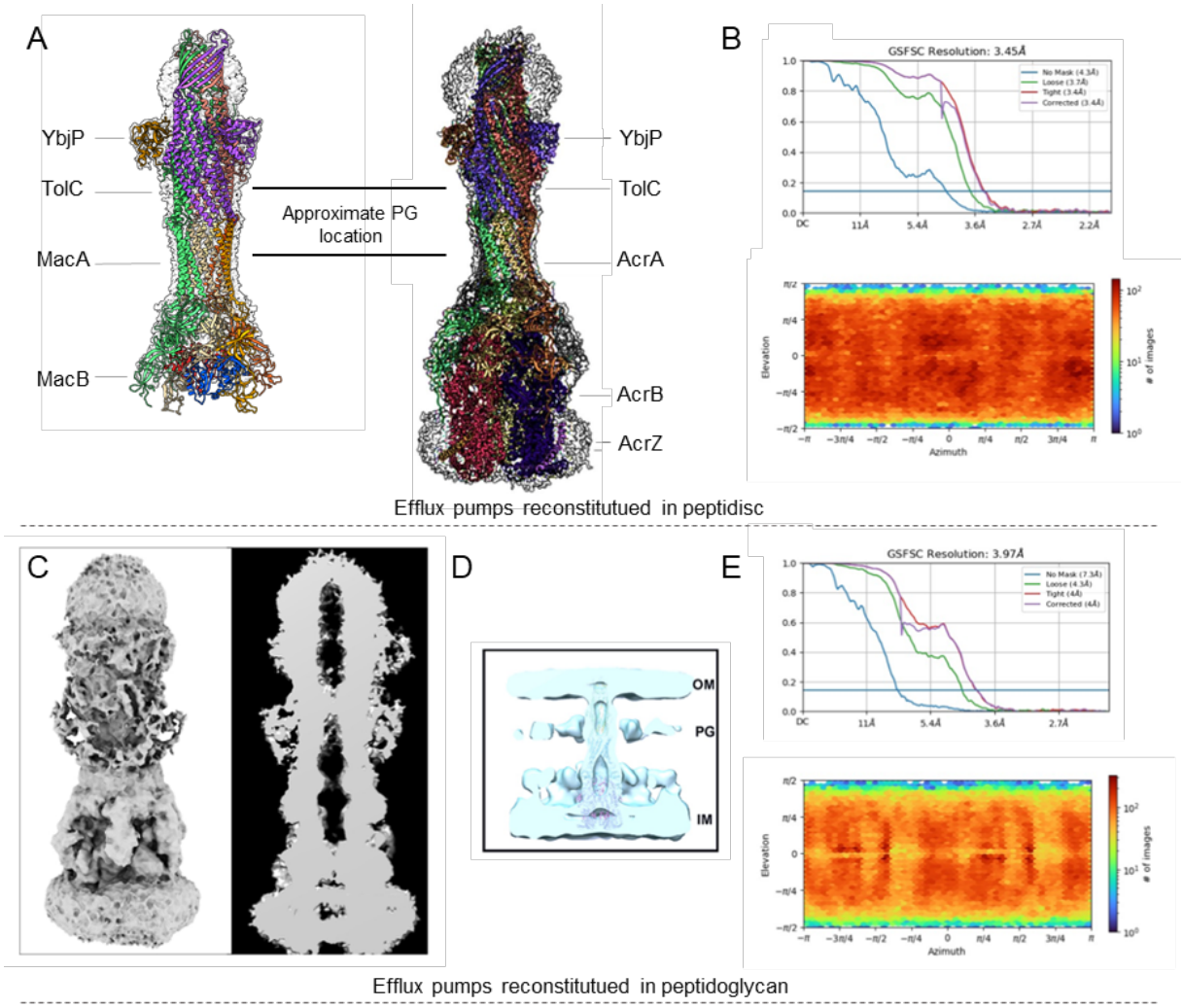

Supplementary Figure S2. YbjP binds at the same position in the AcrABZ-TolC and MacAB-TolC tripartite pumps and may not interact with peptidoglycan. (A) Cryo-EM maps and models of MacAB-TolC-YbjP and AcrABZ-TolC-YbjP reconstituted in peptidisc. (B) Fourier shell correlation between half-maps (*top*) and angular distribution of the particles (*bottom*) for the AcrABZ-TolC-YbjP dataset. (C) Cryo-EM map of AcrABZ-TolC-YbjP reconstituted in peptidoglycan. (D) Peptidoglycan location based on the cryo-ET map described by Shi et al., 2019. A similar location was reported by Gumbert et al., 2020. (E) Fourier Shell Correlation between half-maps (*top*) and angular distribution plot of the particles (*bottom*). Collection statistics for the AcrABZ-TolC-YbjP complex reconstituted in peptidisc and in peptidoglycan are listed in Supplementary Table S2.

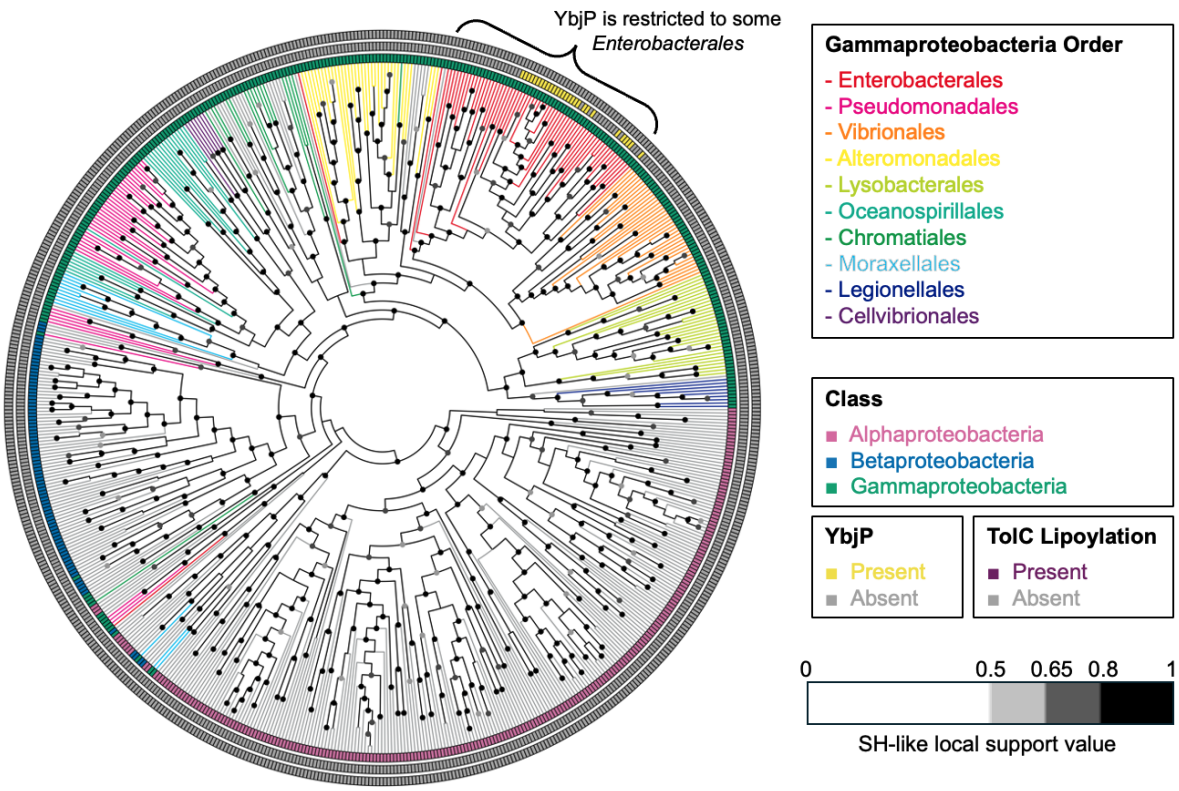

Supplementary Figure S3. The cladogram of TolC (IPR010130) in *Pseudomonadota*. The sequence that showed the highest pairwise similarity to *E. coli* TolC in each organism is selected. None of these TolC proteins contain any lipoylation signal.

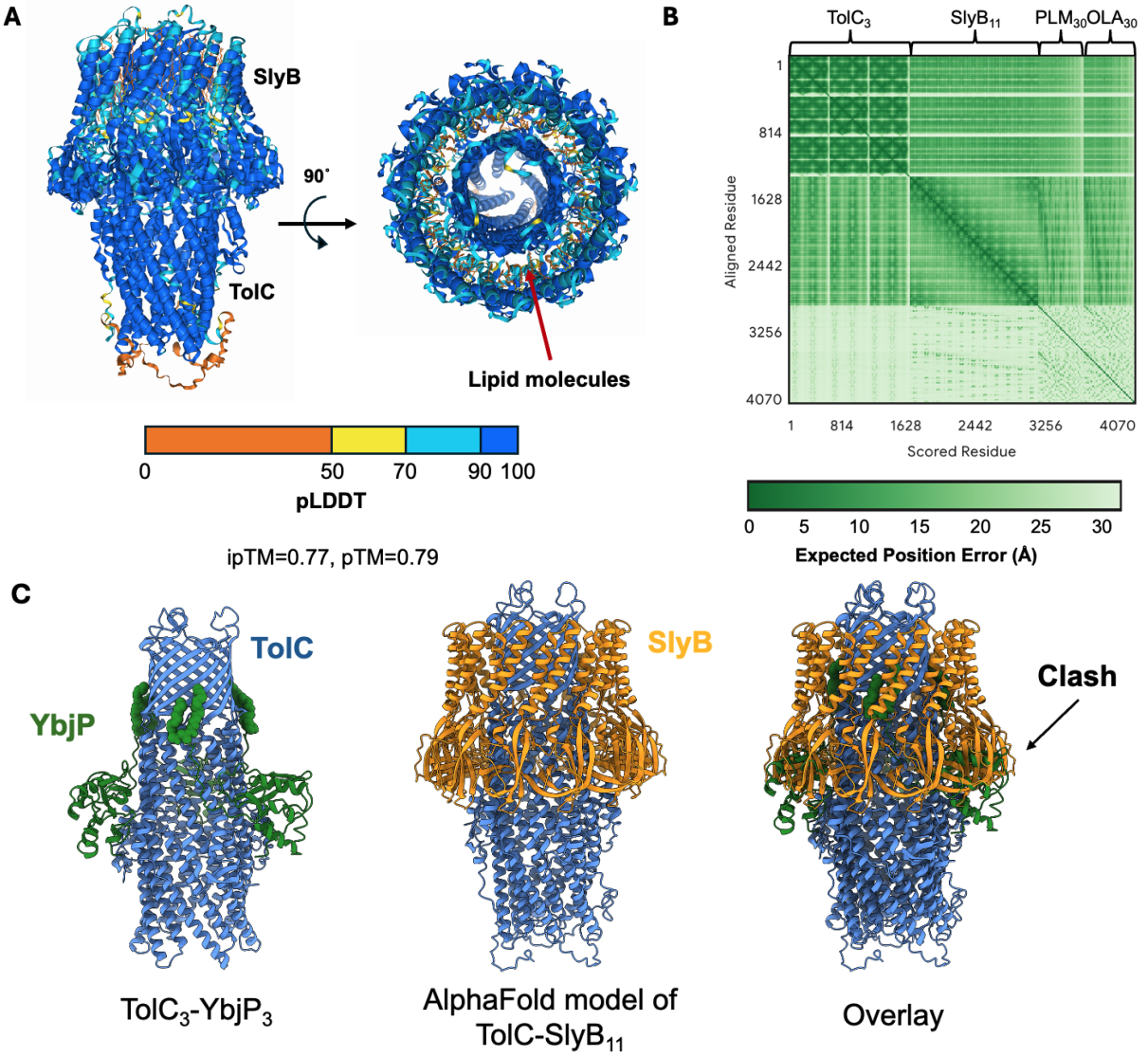

Supplementary Figure S4. Structural comparison of $TolC_3$–$YbjP_3$ and $TolC_3$–$SlyB_{11}$. (A) AlphaFold structure of TolC-$SlyB_{11}$ with 30 palmitic acid (PLM) and 30 oleic acid (OLA) molecules. The model is colored by pLDDT score. The signal peptides of TolC and SlyB are cleaved. (B) PAE plot of $TolC_3$–$SlyB_{11}$ with 30 PLM and 30 OLA molecules. (C) Overlay of $TolC_3$–$YbjP_3$ structure and $TolC_3$–$SlyB_{11}$ AlphaFold structure. The lipoylation in YbjP is displayed as *green* spheres.

Table S1. Cryo-EM data and refinement for MacAB-TolC-YbjP

Protein structure	**MacAB-TolC-YbjP**
Organism	*E. coli*
PDB ID	9QGY
EMDB ID	EMD-53150
Data collection	
Microscope	FEI Titan Krios
Voltage (kV)	300
Detector	K3
Mode	counting, super-resolution
Nominal magnification	105,000 ×
Pixel size (Å/pix)	0.830 (0.415)
Electron fluency, per frame (e^-/Å^2)	0.975
Electron fluency, total (e^-/Å^2)	49.75
Defocus range (µm), step (µm)	–0.8 to –2.7, 0.3
Exposure (s)	1
Frames	51
Number of micrographs	5,399
Reconstruction	
Software	cryoSPARC-4.5.3
Final number of particle images	233,775
Point group	C_3
Map resolution, $FSC_{0.143}$ (Å)	2.48
Map-sharpening B factor (Å^2)	76.6
Model composition	
Non-hydrogen atoms	65193
Protein residues	4198
Ligands (PDB)	
Refinement	
Software	Phenix-1.20
Correlation coefficient, masked	0.84
Correlation coefficient, box	0.61
Model resolution, $FSC_{0.5}$ (Å)	2.4
Validation (proteins)	
MolProbity score	1.48
Clash score, all atoms	6.59
Ramachandran plot statistics	
Favoured, overall (%)	97.4

Table S2. Cryo-EM analysis of AcrABZ-TolC-YbjP

	AcrABZ-TolC-YbjP peptidisc	AcrABZ-TolC-YbjP peptidoglycan
Data collection and processing		
Magnification	100,000x	100,000x
Voltage (kV)	300	300
Electron exposure ($e^-/Å^2$)	56	56
Defocus range (μm)	-1, -2.5	-1, -2.5
Pixel size (Å)	0.723	0.723
Number of Micrographs	13,456	13,456
Symmetry imposed	C1	C1
Initial particle images (no.)	271,642	271,642
Final particle images (no.)	185,112	62,804
Map resolution (Å, FSC = 0.143)	3.45	3.97
Particle box size	540	540

Table S3. ITC parameters for the TolC-YbjP$_s$ interaction

K_D (μM)	N	ΔG	ΔH	-TΔS
4.1, 5.9	0.64, 0.42	-7.4, -7.1	-37.8, -14.3	30.5, 7.15
5.0 ± 1.3	**0.53 ± 0.16**	**-7.3 ± 0.2**	**-26.1 ± 16.6**	**18.9 ± 16.5**

Results were obtained with DDM-purified TolC and the soluble construct of YbjP (residues 28 to 171) removing the tri-acyl moiety. The mean ± standard deviation of two independent repeats is shown in bold. Experiments were carried out at a temperature of 25°C. Values of ΔG, ΔH and TΔS are in kcal mol^{-1}. An example of thermograms and fit is shown in Figure 3B.

Table S4. Criteria for classification of DUF3828-containing proteins

Family	Tai3	YbjP	Alphaproteobacteria
Taxonomy	Betaproteobacteria Gammaproteobacteria Bacteroidota/Chlorobiota group	Enterobacterales under Gammaproteobacteria	Alphaproteobacteria
Gene Synteny	Tae3	Arginine transporter Amidase	Unclear
Signal peptide	Lipoprotein	Either lipoprotein or periplasmic	Periplasmic
QDX motif	Present	Absent	Present